Supporting Information

Tailoring the Hydrophobicity and Zincophilicity of Poly(ionic liquid)s Solid-electrolyte Interphases for Ultra-stable Aqueous Zinc Batteries

1. Experimental Details

Synthesis of 3-(1-vinyl-3-imidazolio) propanesulfonate (VIPS)

[VIPS] was synthesized using a previously reported method.[1, 2] 9.41 g 1-vinylimidazole (99%, Aladdin) was dissolved in 60 mL of acetone. Then an equimolar amount of 1,3-propanesultone (99%, Aladdin) dissolved in 40 mL of acetone was added dropwise to the above solution at 0 °C under a nitrogen atmosphere. After stirred for 3 days at room temperature, the resultant solid was filtered and washed with acetone at least three times. Finally, the obtained VIPS was dried under vacuum at room temperature.

Synthesis of 3-(1-vinyl-3-imidazolio) propanesulfonate ([VIPS][Zn(TFSI)$_2$])

$Zn(TFSI)_2$ was bound to [VIPS] via electrostatic interaction between $-SO_3^-$ and Zn^{2+} to synthesize [PVIPS][$Zn(TFSI)_2$]. 3-(1-vinyl-3-imidazolio) propanesulfonate (VIPS) and $Zn(TFSI)_2$ (98%, Aladdin) was dissolved in moderate amounts of methanol respectively. Then the solution with $Zn(TFSI)_2$ was slowly dripped into VIPS solution using a constant pressure drip funnel at room temperature. After stirring for 24 h, vacuum spin steam and place in vacuum drying oven for 72 h. [VIPS][$Zn(TFO)_2$] and [VIPS][$Zn(BF_4)_2$] were synthesized by replacing $Zn(TFSI)_2$ with $Zn(TFO)_2$ (98%, Aladdin) and $Zn(BF_4)_2$ (98%, Aladdin) in the same way.

Preparation of casting solution

3wt% PIL monomer, 1wt% crosslink PEGDA, and 0.1wt% photoinitiator E1173 were dissolved in metha nol to obtain the casting solution.

Preparation of [PVIPS][Zn(TFSI)$_2$]@Zn and [PVBIm][TFSI]@Zn electrodes

The casting solution was dripped onto the zinc foil (about 88.50μL·cm^{-2}) and polymerized 40 min under 365 nm ultraviolet light. Then the coated zinc foil was kept at room temperature for 2 h to completely volatilize the solvent and get the [PVIPS][$Zn(TFSI)_2$]@Zn and [PVBIm][TFSI]@Zn electrodes.

Preparation of polyaniline (PANI) cathodes

Cathodes were prepared in N-methylpyrrolidone (NMP, 99%, J&K Scientific) by mixing polyaniline (98%, Macklin), polyvinylidene fluoride (PVDF, Aladdin), acetylene black, carbon nanotube (CNT, 95%, Aladdin) (7:1:1:1 by weight). The slurry was rolled and pressed onto the carbon paper, followed by drying in a vacuum oven at 80 °C overnight. The mass loading of PANI in the cathode was ~1.7 mg·cm^{-2}.

Material Characterization

Scanning Electron Microscopy (SEM) images were obtained using a scanning electron microscope (Gemini SEM300) operating at 10 kV using tungsten filament as the electron source. X-ray diffraction (XRD) patterns of the powders and membranes were obtained by a Rigaku SmartLab 9 kW X-ray diffractometer (Cu Kα radiation). X-ray photoelectron spectroscope (XPS) patterns were obtained by Thermo Scientific K-Alpha (Al Kα radiation). Fourier transform infrared were tested by FT-IR (Bruker ALPHA Ⅱ). The wettability of the electrodes was studied by contact angle goniometer (Kruss DSA100S).

Electrochemical measurements

The electrochemical tests were evaluated using CR2032 coin cells assembled in the air using glass fiber separator. 2 M $ZnSO_4$ electrolyte was applied as electrolyte for all tests. For the symmetric cells, two pieces of bare Zn foils (or [PVIPS][$Zn(TFSI)_2$]@Zn, [PVBIm][TFSI]@Zn) were served as electrodes. For the half cells, Ti foils were used as cathodes. For the full cells, the cathodes were replaced by PANI.

Galvanostatic charge-discharge tests were carried out on a LAND instrument (CT3002A). Electrochemical impedance spectra (EIS), chronoamperograms, cyclic voltammetry (CV), and linear polarization curves (LSV) were collected on an electrochemical analyzer (CHI 760D).

2. Supplementary figures

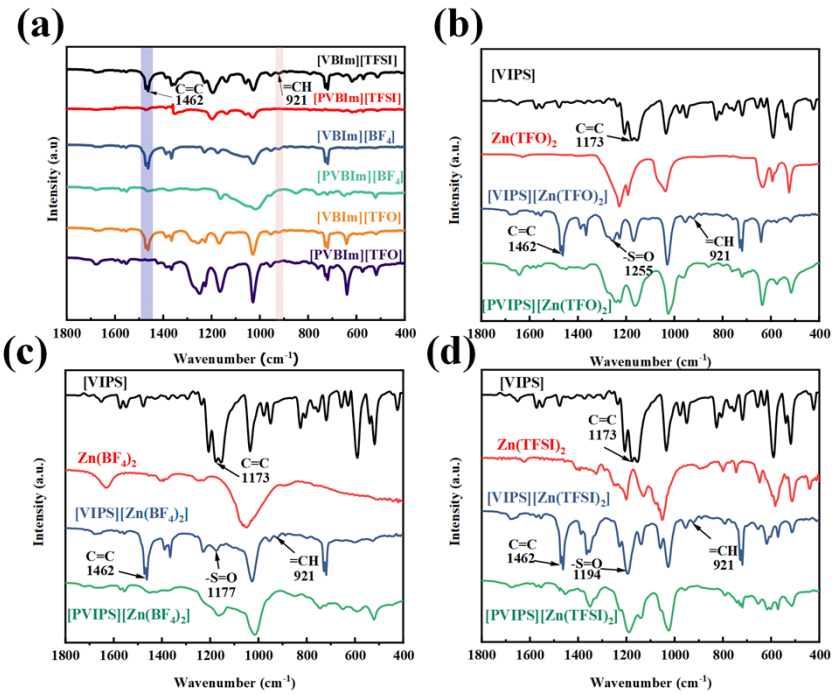

Figure S1. FTIR spectrum of (a) [VBIm][TFSI], [PVBIm][TFSI], [VBIm][BF_4], [PVBIm][BF_4], [VBIm][TFO], [PVBIm][TFO]; (b) VIPS, $Zn(TFO)_2$, [VIPS][$Zn(TFO)_2$], [PVIPS][$Zn(TFO)_2$]; (c) VIPS, $Zn(BF_4)_2$, [VIPS][$Zn(BF_4)_2$], [PVIPS][$Zn(BF_4)_2$]; and (d) VIPS, $Zn(TFSI)_2$, [VIPS][$Zn(TFSI)_2$], [PVIPS][$Zn(TFSI)_2$].

As shown in Figure S1a, it is evident that [VBIm][TFSI] displays distinct tensile stretching vibration at 1462 cm^{-1} and =CH bending vibration at 921 cm^{-1}. However, these peaks noticeably decrease on the zinc surface after in-situ polymerization. This observation substantiates that the hydrophobic layer predominantly comprises a polymer resulting from the breaking and polymerization of carbon-carbon double bonds within [VBIm][TFSI]. The structural diagram and molecular formula of the [PVBIm][TFSI] layer are depicted in Figure 1A. As for the construction of the [PVIPS][$Zn(TFSI)_2$] layer, it involves two main steps. The initial step entails the formation of [VIPS][$Zn(TFSI)_2$] via the interaction between the $-SO_3^-$ of VIPS and Zn^{2+} from $Zn(TFSI)_2$. The presence of C=C and =CH peaks in the infrared spectrum, along with the shift in the -S=O group, serves as evidence of successful synthesis. Subsequently, the [VIPS][$Zn(TFSI)_2$] undergoes polymerization on the zinc surface to form [PVIPS][$Zn(TFSI)_2$] layer. The absence of C=C and =CH signals in the coating conclusively verifies success polymerization of the SEI layer. The structure and composition of this [PVIPS][$Zn(TFSI)_2$] layer are illustrated in Figure 1b.

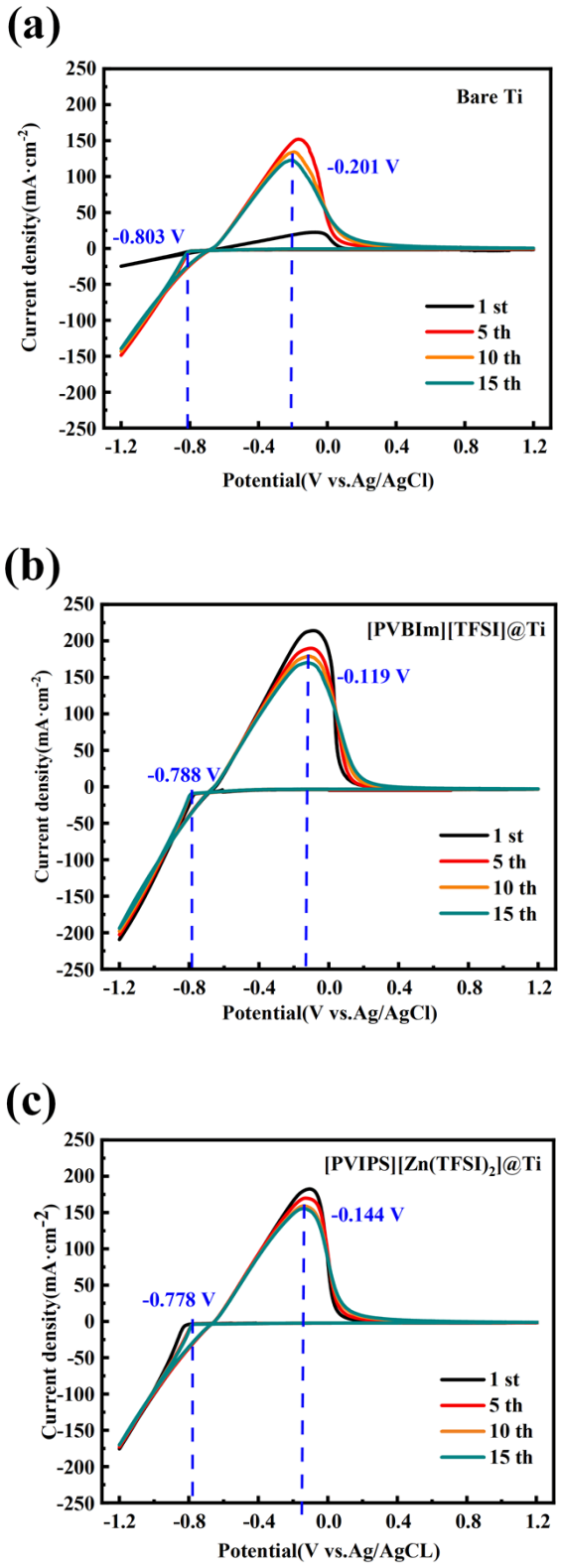

Figure S2. Cyclic voltammetry test in three-electrode system with (a) bare Ti, (b) [PVBIm][TFSI]@Ti, and (c) [PVIPS][Zn(TFSI)$_2$]@Ti as working, Zn as counter, and Ag/AgCl as reference electrode at scan rate of 50 mV·s^{-1}.

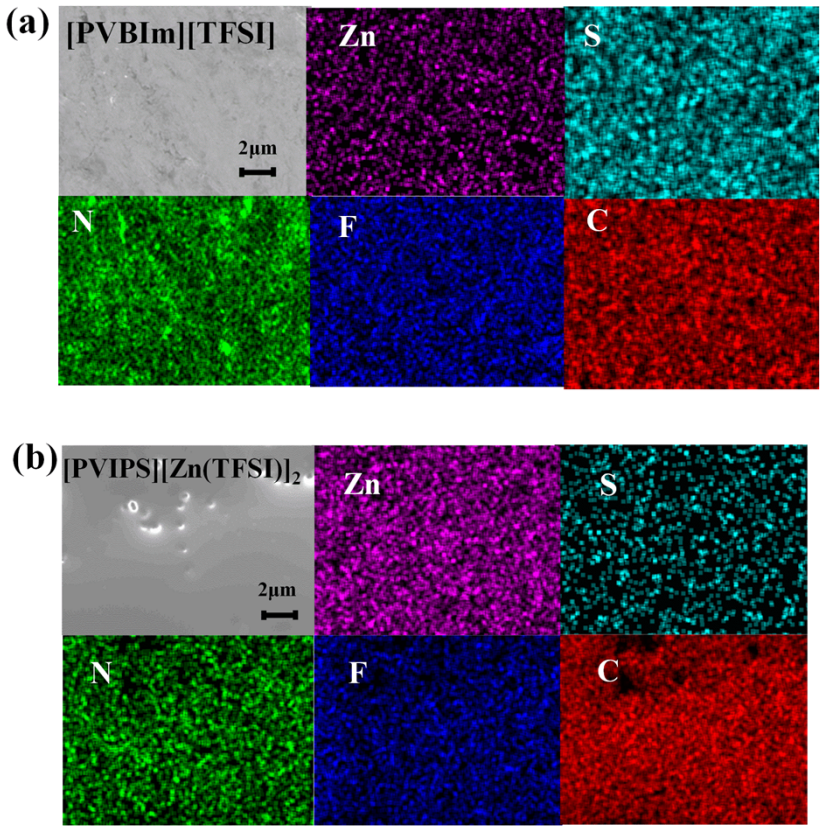

Figure S3. SEM images of (a) [PVBIm][TFSI]@Zn and (b) [PVIPS][$Zn(TFSI)_2$]@Zn with corresponding EDS mapping results.

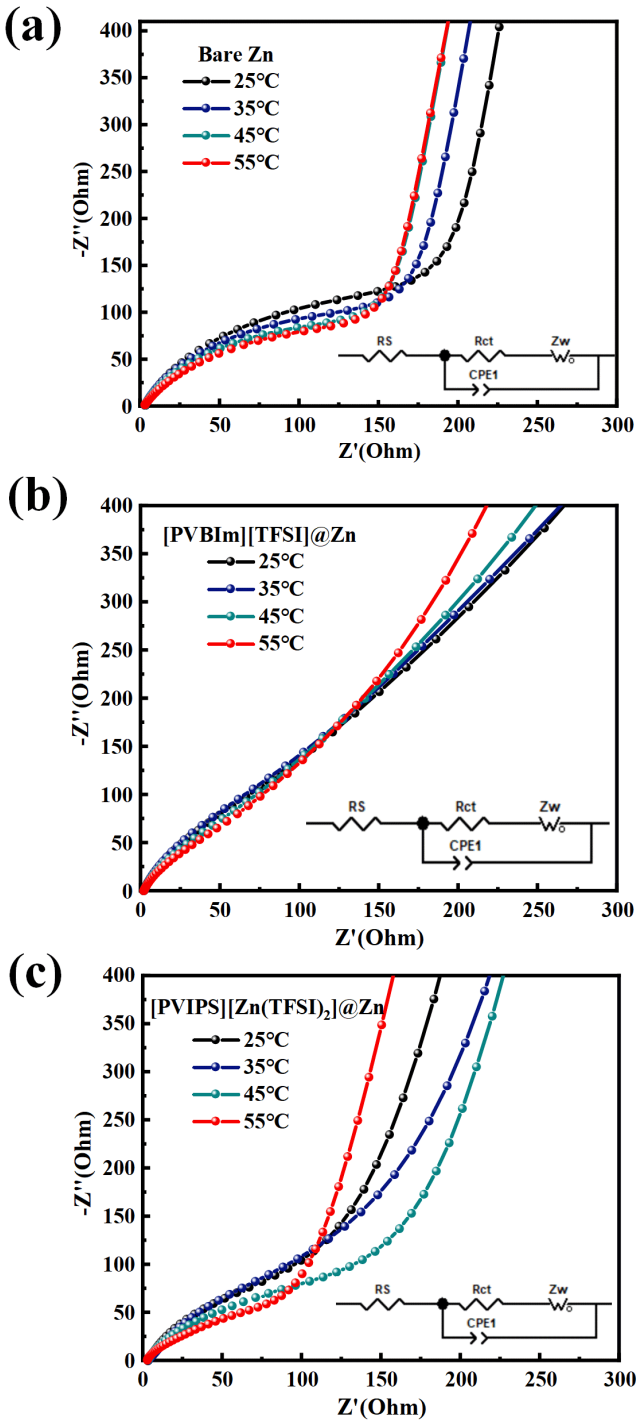

Figure S4. Nyquist plot of (a) Bare Zn, (b) [PVBIm][TFSI]@Zn, and (c) [PVIPS][Zn(TFSI)$_2$]@Zn symmetrical cells at 25°C-55°C.

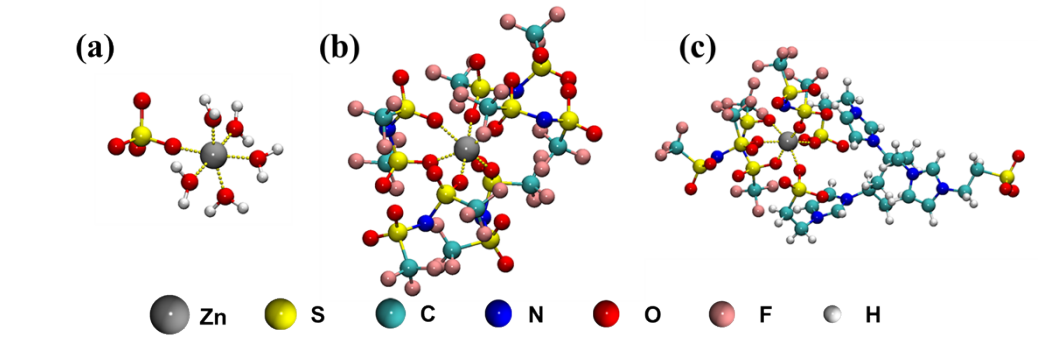

Figure S5. Schematic of the coordination structures of Zn^{2+} in (a) $ZnSO_4$ aqueous electrolyte, (b) [PVBIm][TFSI] SEI, and (c) [PVIPS][$Zn(TFSI)_2$] SEI.

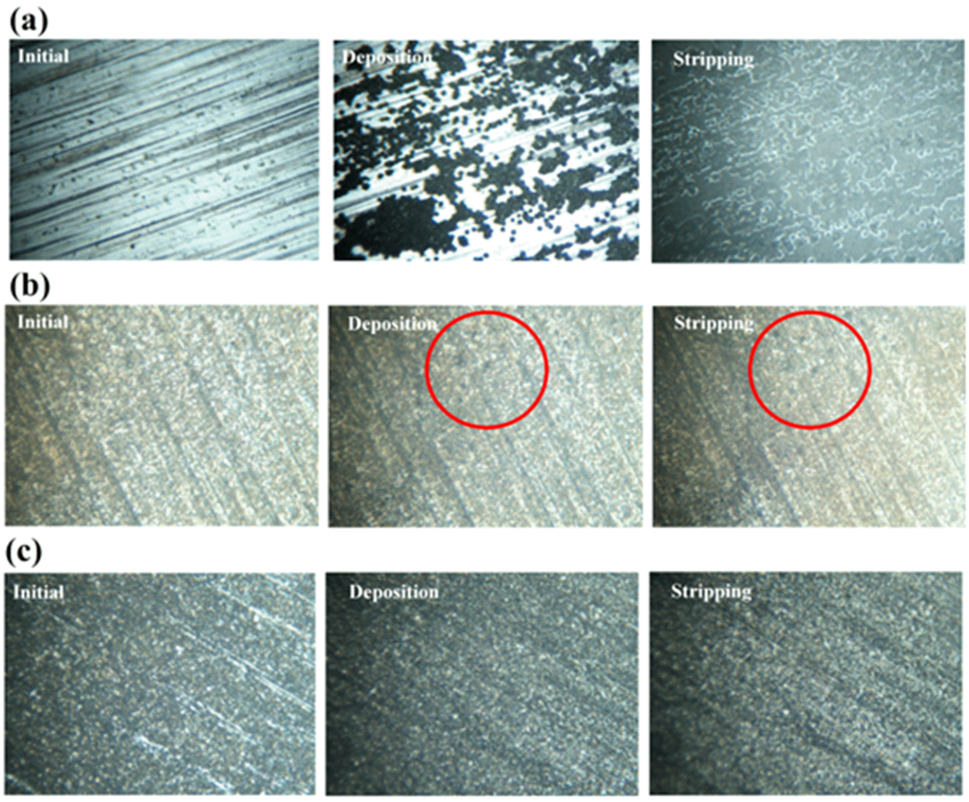

Figure S6. Top-view in-situ optical microscope observation of Zn plating/stripping processes for (a) Bare Zn, (b) [PVBIm][TFSI]@Zn, and (c) [PVIPS][Zn(TFSI)$_2$]@Zn.

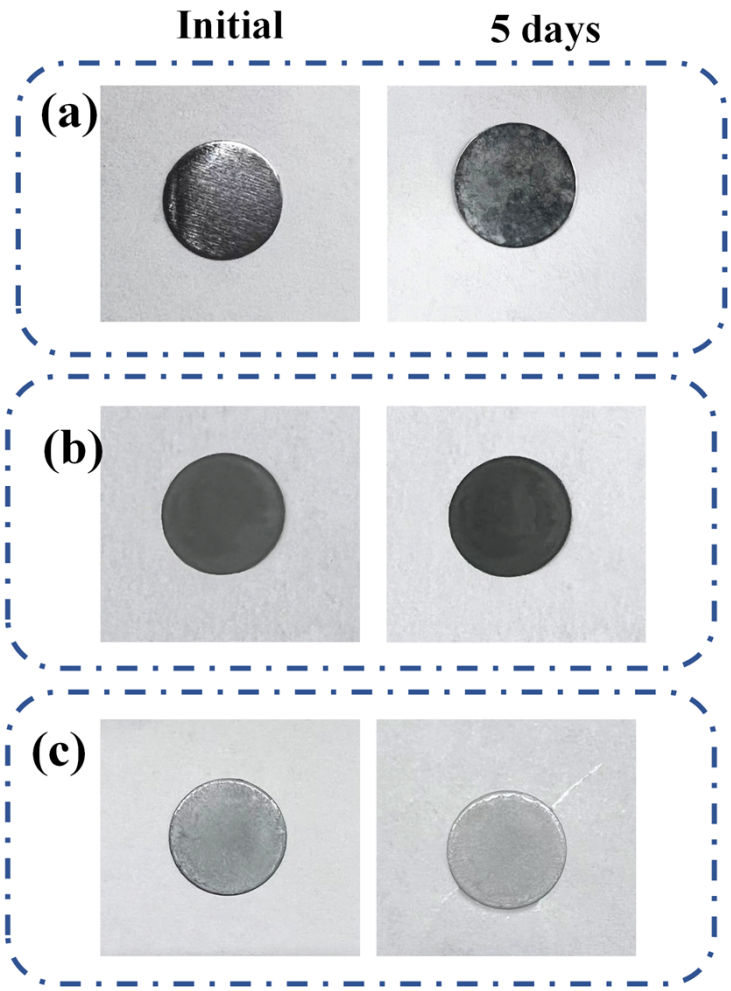

Figure S7. Photos of (a) bare Zn, (b) [PVBIm][TFSI]@Zn, and (c) [PVIPS][Zn(TFSI)$_2$]@Zn soaked in 2M $ZnSO_4$ for 5 days at 25°C.

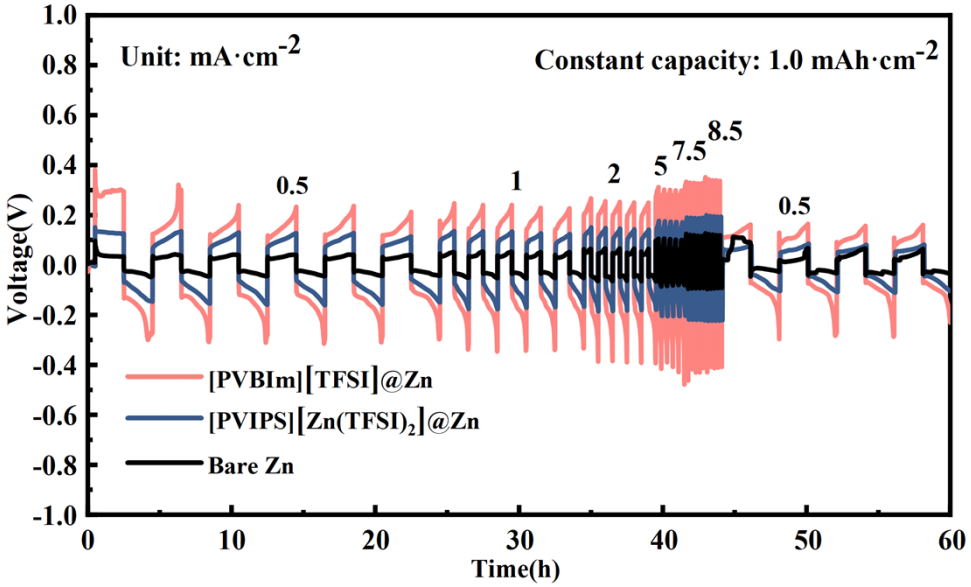

Figure S8. Rate performance of bare Zn, [PVBIm][TFSI]@Zn, and [PVIPS][$Zn(TFSI)_2$]@Zn symmetrical cells at a fixed capacity of 1.0 $mAh \cdot cm^{-2}$.

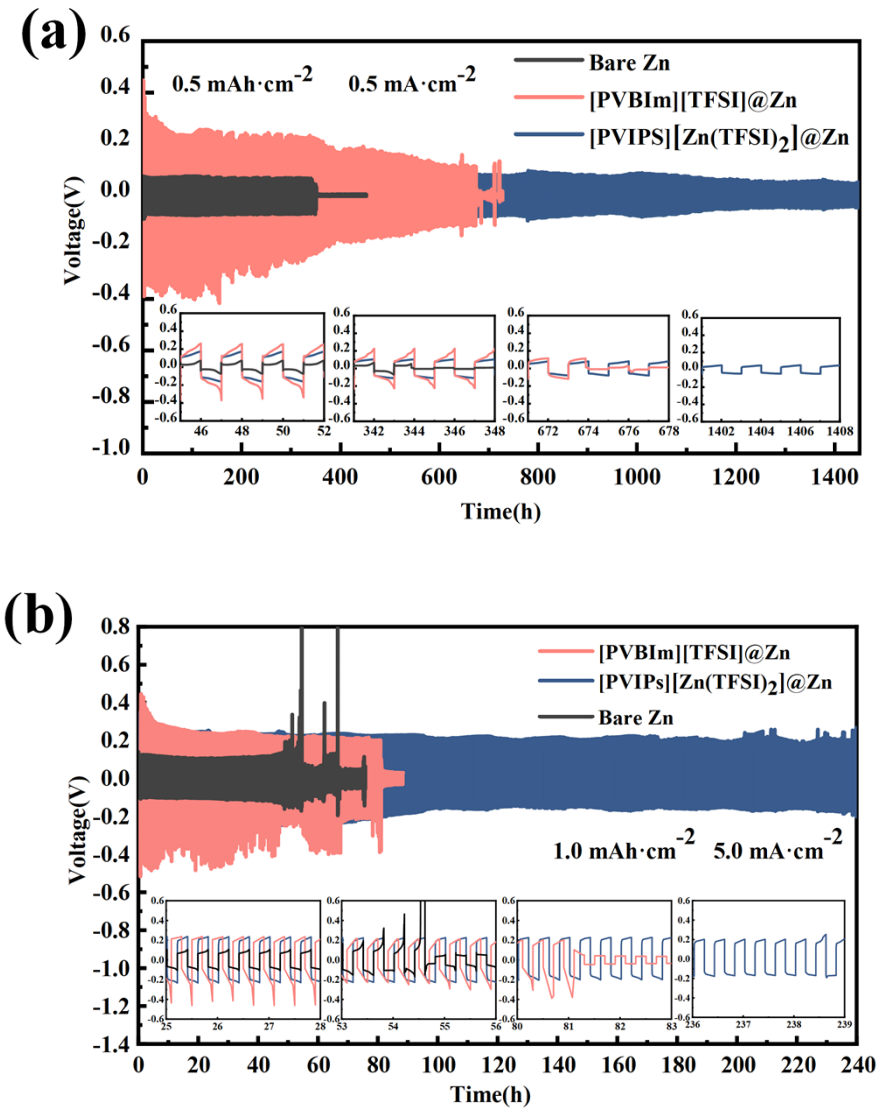

Figure S9 Galvanostatic cycling of bare Zn, [PVBIm][TFSI]@Zn, and [PVIPS][$Zn(TFSI)_2$]@Zn symmetric cells at current densities of (a) 0.5 mA·cm^{-2}/0.5 mAh·cm^{-2} and (b) 5.0 mA·cm^{-2}/1.0 mAh·cm^{-2}.

3. Supplementary tables.

Table S1. Cycling performance of the Zn symmetrical cells with different SEIs.

Composition of SEI	Coulomb efficiency (%)	Cycle life (h)	Reference
[PVBIm][TFSI]	99.6 (0.5 mA·cm^{-2})	675 (0.5 mA·cm^{-2})	This work
[PVIPS][Zn(TFSI)$_2$]	98.0 (0.5 mA·cm^{-2})	1950 (1.0 mA·cm^{-2})	This work
TMPMP-TMPTA-BMPTFSI IL gel	96.6 (0.5 mA·cm^{-2})	1000 (0.1 mA·cm^{-2})	[3]
Poly (ether ether ketone)	98.0 (1.0 mA·cm^{-2})	500 (1.0 mA·cm^{-2})	[4]
1,3,5,9-Tetrathiophenylpyrene	98.4 (0.885 mA·cm^{-2})	1000 (0.885 mA·cm^{-2})	[5]
(LCNF)-MXene	98.9 (1.0 mA·cm^{-2})	800 (1.0 mA·cm^{-2})	[6]
rich-cyano SEI	99.65 (1.0 mA·cm^{-2})	500 (1.0 mA·cm^{-2})	[7]
acrylic-bonded stationary	99.9 (1.0 mA·cm^{-2})	1000 (1.0 mA·cm^{-2})	[8]
Nafion-Zn-X zeolite nanoparticles	97.0 (1.0 mA·cm^{-2})	1000 (1.0 mA·cm^{-2})	[9]
$Zn(H_2PO_4)_2$	99.4 (1.0 mA·cm^{-2})	800 (0.5 mA·cm^{-2})	[10]
$Zn_5(OH)_8(NO_3)_2 \cdot 2H_2O$	99.8 (0.5 mA·cm^{-2})	1200 (0.5 mA·cm^{-2})	[11]
ATMP-Zr (AZ)	99.5 (1.0 mA·cm^{-2})	1800 (1.0 mA·cm^{-2})	[12]

Reference

1. F. Lu, G. Li, Y. Yu, X. Gao, L. Zheng and Z. Chen, *Chemical Engineering Journal*, 2020, **384**, 123237.
2. G. Garg, G. S. Chauhan, R. Gupta and J. H. Ahn, *Journal of Colloid and Interface Science*, 2010, **344**, 90-96.
3. D. Lee, H.-I. Kim, W.-Y. Kim, S.-K. Cho, K. Baek, K. Jeong, D. B. Ahn, S. Park, S. J. Kang and S.-Y. Lee, *Advanced Functional Materials*, 2021, **31**, 2103850.
4. Q. Jian, Y. Wan, Y. Lin, M. Ni, M. Wu and T. Zhao, *ACS Applied Materials & Interfaces*, 2021, **13**, 52659-52669.
5. X. Qi, F. Xie, Y.-T. Xu, H. Xu, C.-L. Sun, S.-H. Wang, J.-Y. Hu and X.-F. Wang, *Chemical Engineering Journal*, 2023, **453**, 139963.
6. C. Liu, Z. Li, X. Zhang, W. Xu, W. Chen, K. Zhao, Y. Wang, S. Hong, Q. Wu, M.-C. Li and C. Mei, *Advanced Science*, 2022, **9**, 2202380.
7. H. Yan, C. Han, S. Li, J. Liu, J. Ren, S. Yang and B. Li, *Chemical Engineering Journal*, 2022, **442**, 136081.
8. C. Huang, W. Deng, X. Yuan, Y. Zhou, C. Li, J. Hu, M. Zhang, J. Zhu and R. Li, *ACS Applied Materials & Interfaces*, 2023, **15**, 2341-2350.
9. Y. Cui, Q. Zhao, X. Wu, X. Chen, J. Yang, Y. Wang, R. Qin, S. Ding, Y. Song, J. Wu, K. Yang, Z. Wang, Z. Mei, Z. Song, H. Wu, Z. Jiang, G. Qian, L. Yang and F. Pan, *Angewandte Chemie International Edition*, 2020, **59**, 16594-16601.
10. X. Zeng, J. Mao, J. Hao, J. Liu, S. Liu, Z. Wang, Y. Wang, S. Zhang, T. Zheng, J. Liu, P. Rao and Z. Guo, *Advanced Materials*, 2021, **33**, 2007416.
11. D. Li, L. Cao, T. Deng, S. Liu and C. Wang, *Angewandte Chemie International Edition*, 2021, **60**, 13035-13041.
12. J. Ren, C. Li, P. Li, S. Liu and L. Wang, *Chemical Engineering Journal*, 2023, **462**, 142270.